

Extraction of the Heavy-Quark Potential from Bottomonium Observables in Heavy-Ion Collisions

Xiaojian Du, Shuai Y.F. Liu and Ralf Rapp

Cyclotron Institute and Department of Physics and Astronomy, Texas A&M University, College Station, Texas 77843-3366, USA

Abstract

The in-medium color potential is a fundamental quantity for understanding the properties of the strongly coupled quark-gluon plasma (sQGP). Open and hidden heavy-flavor (HF) production in ultrarelativistic heavy-ion collisions (URHICs) has been found to be a sensitive probe of this potential. Here we utilize a previously developed quarkonium transport approach in combination with insights from open HF diffusion to extract the color-singlet potential from experimental results on Υ production in URHICs. Starting from a parameterized trial potential, we evaluate the Υ transport parameters and conduct systematic fits to available data for the centrality dependence of ground and excited states at RHIC and the LHC. The best fits and their statistical significance are converted into a temperature dependent potential. Including nonperturbative effects in the dissociation rate guided from open HF phenomenology, we extract a rather strongly coupled potential with substantial remnants of the long-range confining force in the QGP.

Keywords: Quark-Gluon Plasma, Heavy-Quark potential, Bottomonium

PACS: 12.39.Pn, 25.75.-q, 12.38.Mh

1. Introduction

The confining force of Quantum Chromodynamics (QCD) plays a central role in the quantitative description of the bound-state spectra of charmonia and bottomonia in vacuum [1], characterized by a linear term in color-singlet potential between a color charge and its anti-charge. It has also been applied rather successfully for light hadrons [2, 3] (with caveats in the chiral sector). Thus, the in-medium properties of quarkonia have long been recognized as promising probe for the formation of the quark-gluon plasma (QGP) in ultrarelativistic heavy-ion collisions (URHICs) [4–9]. In addition, the consequences of in-medium potentials on heavy-quark (HQ) diffusion [10–12] and QGP structure [13–18] have been studied, where remnants of the confining force above the pseudo-critical temperature, T_{pc} , were found to be essential in explaining the properties of the strongly-coupled QGP (sQGP). Recent efforts to define the potential [19–21] and relate it to quantities computed in IQCD, such as the free energy or quarkonium correlators, made progress in extracting this potential [22–24]. In these approaches the HQ free (F) and internal (U) energies, previously used as potential proxies, are rather outputs of suitably defined interaction

kernels. However, the present results are not unique, ranging from a weak potential [18, 23], close to F , to a stronger one [18, 24, 25], close to the vacuum potential at moderate QGP temperatures.

Transport analyses of open and hidden heavy-flavor (HF) production in URHICs require relatively strong interaction potentials for heavy-light and heavy-heavy interactions, respectively. For example, low-momentum D -meson observables (in particular their elliptic flow) clearly favor the U -potential over the F -potential proxy [11, 12] (or require large K factors when using perturbative interactions [26]); similar trends are found for quarkonium observables in URHICs [27–31] albeit systematic constraints have not been evaluated yet. Bottomonium observables are particularly promising to achieve that. Theoretically, the large bottom-quark mass renders the potential approach most suitable; phenomenologically, regeneration contributions are expected to be smaller [29] than in the charmonium sector where they reduce the sensitivity to the underlying potential [27]; experimentally, the recent increase in available data and their precision, encompassing both ground ($\Upsilon(1S)$) and excited states ($\Upsilon(2S)$, $\Upsilon(3S)$) at RHIC [32, 33] and the LHC [34–38] has reached a point where a quantitative sensitivity to the in-medium poten-

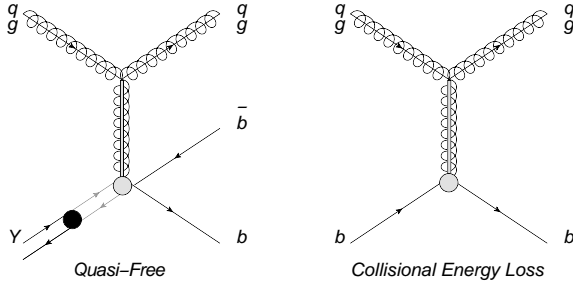


Figure 1: Relation between “quasifree” dissociation of quarkonia and single HQ interactions in the QGP. The vertical lines represent the in-medium potential between thermal partons and heavy quark(onium).

tial seems possible [39].

In the present work, we conduct a statistical analysis of the centrality dependence of available bottomonium data at RHIC and the LHC, with the goal of constraining the HQ potential at finite temperature. Toward this end, we employ our previously developed semi-classical Boltzmann/rate equation approach which has been extensively tested by a wide variety of quarkonium observables from SPS via RHIC to LHC energies for both charmonia and bottomonia [27, 39–41]. Its results are largely consistent with other semi-classical approaches [28, 30, 42–47], although quantitative cross comparisons under controlled conditions remain to be carried out [9]. Furthermore, the effects of explicit quantum evolution equations for quarkonia are receiving increased attention [48–52]. However, it has not yet been scrutinized in how far quantum effects affect the extraction of transport parameters, and most of the pertinent calculations do not yet employ realistic potentials including the string term, which plays a critical role in the dissociation processes even for bottomonia. The implications for the systematic uncertainty of semi-classical approaches will have to be elaborated in future work.

The key connection between the in-medium potential and quarkonium transport is the inelastic reaction rate which increases as the potential weakens. In practice, inelastic parton ($i = q, \bar{q}, g$) scattering of the type $i + Y \rightarrow i + b + \bar{b}$ has been identified as the leading contribution to the dissociation rate in the relevant regime of temperatures where the dissociation energies are relatively small (also referred to as an imaginary part of the HQ potential [19–21], or “quasifree dissociation” [53]). Since the basic diagrams essentially correspond to heavy-light scattering, $i + b \rightarrow i + b$, they are closely related to HQ diffusion, cf. Fig. 1. From HF phenomenology it is now well established that HQ

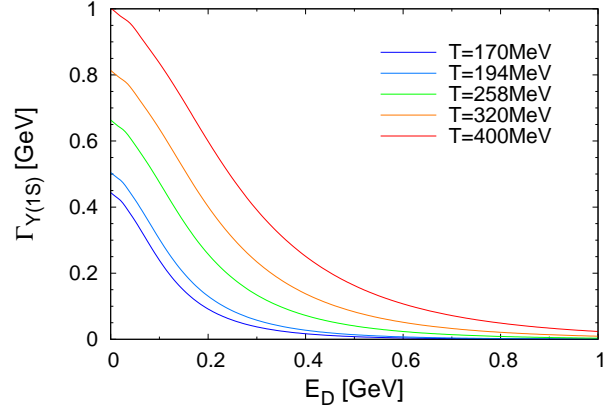


Figure 2: Dissociation energy dependence of the quasifree width (with $K=5$) for a fixed Y mass of 9.46 GeV at different temperatures.

transport coefficients require a large enhancement over perturbative results [12, 26]. Reliable extractions of the in-medium HQ potential in quarkonium transport have to account for this.

2. Y Transport and in-Medium Potential

The quarkonium transport framework employed in this work utilizes a rate equation [27, 39, 40],

$$\frac{dN_Y(\tau)}{d\tau} = -\Gamma(T(\tau)) [N_Y(\tau) - N_Y^{\text{eq}}(T(\tau))], \quad (1)$$

for the number, N_Y , of different bottomonia, $Y = \Upsilon(1S), \Upsilon(2S), \Upsilon(3S), \chi_b(1P)$. The equilibrium limit, $N^{\text{eq}}(T)$, governs regeneration processes and is obtained from the thermal model with experimental input for open-bottom cross sections (we also include a relaxation time correction for incomplete b -quark thermalization and correlation volume effects in the canonical ensemble). However, the regeneration contribution to bottomonia is relatively small, and $N^{\text{eq}}(T)$ depends only weakly on the potential through the b and Y masses.

The central quantity is the inelastic reaction rate, $\Gamma(T)$, which depends on temperature through the thermal-parton density and the Y dissociation energy, E_D , which controls the final-state phase space of the dissociation process, cf. Fig. 2.¹ The main contribution to the rate stems from quasifree dissociation [53,

¹Note that, especially in the presence of a long-range string interaction, E_D is not necessarily identical to the binding energy; for example, for the Y ground state in vacuum, its binding may not be strongly affected by the string interaction, but E_D , determined by the $B\bar{B}$ -meson threshold, directly depends on it. In the present paper, we therefore use the notion of dissociation energy as the relevant quantity for calculating reaction rates.

54] for which we include interference effects causing a r -dependent reduction of the widths increasing with the dissociation energy of the bound state [39]. The much smaller contributions to the rate from gluodissociation [55, 56] are also accounted for. A significant extension over our previous work [39] is the implementation of constraints from open HF phenomenology, which require HQ scattering rates in the QGP well beyond perturbative estimates. This is done by introducing a K factor in the quasifree reaction rate, which for simplicity we assume to be temperature- and momentum-averaged. In the presence of large dissociation widths, the issue of the onset temperature for regeneration reactions needs to be revisited, *i.e.*, at what temperature in the cooling of the fireball bound-state formation commences. In our previous work, where the quasifree rates were relatively small, the default assumption was to use the vanishing of the dissociation energy, $E_D^Y(T_{\text{reg}})=0$, to define the temperature, T_{reg} , below which regeneration sets in. However, for dissociation energies much smaller than the width (for a large K factor), the formation time of the bound state becomes longer than its lifetime. Therefore, we amend the criterion for T_{reg} by defining it as the temperature where the dissociation energy becomes comparable to the reaction rate, $E_D^Y(T_{\text{reg}})=\Gamma_Y(T_{\text{reg}})$ (as it turns out, both criteria lead to virtually identical results for the extracted potentials, with some difference in the composition of primordial and regeneration components for excited states). Above T_{reg} the dissociation of would-be quarkonia (*i.e.*, primordially produced $b\bar{b}$ quarks that in a pp collision would evolve into a quarkonium bound state) is still operative at a rate of twice the collision rate of a single b quark. A more rigorous treatment of these issues requires a quantum evolution approach which we defer to future work.

The key quantity to calculate the in-medium dissociation energies is the in-medium potential $V(r, T)$ for which we adopt a screened Cornell-type potential. For an efficient use in the statistical analysis discussed below, we utilize a 2-parameter ansatz for the T -dependence of the potential (akin to that in Ref. [57]), with a Debye screened color-Coulomb term and a confining term whose screening is controlled by a string breaking distance, R_{SB} ,

$$V_{Q\bar{Q}}(r) = \begin{cases} -\frac{4}{3}\alpha_s e^{-m_D r}/r + \sigma r & , r < R_{\text{SB}} \\ -\frac{4}{3}\alpha_s e^{-m_D r}/r + \sigma R_{\text{SB}} & , r > R_{\text{SB}} \end{cases} \quad (2)$$

Here, m_D and $m_S \equiv 1/R_{\text{SB}}$ are the pertinent screening masses. We have checked that the sharp-cutoff version of the string term closely resembles the results for disso-

ciation energies from more elaborate smooth versions as used, *e.g.*, in Refs. [11, 18]. Its advantages are an analytical evaluation of its partial-wave expansion (which can be done analytically) and the dependence on a single parameters (whose temperature dependence, however, turns out to be more involved). For a given potential the dissociation energies are obtained from a T -matrix equation and subsequently serve as input into the reaction rate. In the spirit of the semi-classical Boltzmann approach, they are computed in the narrow-width approximation, while the width effects (including interference) are represented by the reaction rates.

3. Statistical Approach

To implement the in-medium potential into a statistical analysis of bottomonium data within our transport framework, we parameterize the temperature dependence of the screening masses. Guided by previous studies of the potential model within the T -matrix approach, we utilize a constant strong-coupling constant, α_s , and string tension, σ , together with a Debye mass linear in temperature, while the screening of the string term requires more flexibility. We make the ansätze

$$m_D = aT_o\tilde{T}, \quad (3)$$

$$m_S = m_S^{\text{vac}} + T_o \left[c\tilde{T} - (c-b) \left(\sqrt{\tilde{T}^2 + d^2} - d \right) \right], \quad (4)$$

where $m_S^{\text{vac}} \simeq 1/\text{fm}$ is the inverse string-breaking distance in vacuum and $\tilde{T} = \frac{T}{T_o} - 1$ is the “reduced” temperature relative to the onset temperature of screening. The four dimensionless fit parameters characterize the slope of m_D (a), the high- T and low- T slopes of m_S (b and c , respectively), and the transition between the two (d); *e.g.*, for $d=0$, the low- T slope drops out. The in-medium b -quark mass includes a self energy from the potential [11, 18], $m_b = m_b^0 + \frac{1}{2} \left(-\frac{4}{3}\alpha_s m_D + \frac{\sigma}{m_S} \right)$, where m_b^0 is the bare mass. With $m_b^0=4.719$ GeV, $\alpha_s=0.298$, $\sigma=0.220$ GeV² and $m_S^{\text{vac}}=0.194$ GeV a good fit to the vacuum masses of $\Upsilon(1S)$, $\Upsilon(2S)$, $\chi_b(1P)$ and $\chi_b(2P)$ is obtained. The values for α_s and σ obtained through our fit are consistent with LQCD results [58–60] at the scales relevant for bottomonia. For the onset temperature of screening, our default value is $T_o=0.15$ GeV, slightly below the QCD pseudo-critical temperature. Guided by LQCD data [61] for the infinite-distance limit of the HQ free energy below T_{pc} , we have also checked a smaller value of $T_o=0.13$ GeV, but did not find significant differences in the final results for the extracted in-medium potential (as we will see below, the screening of the string term turns out to be small up to $T \simeq 0.2$ GeV).

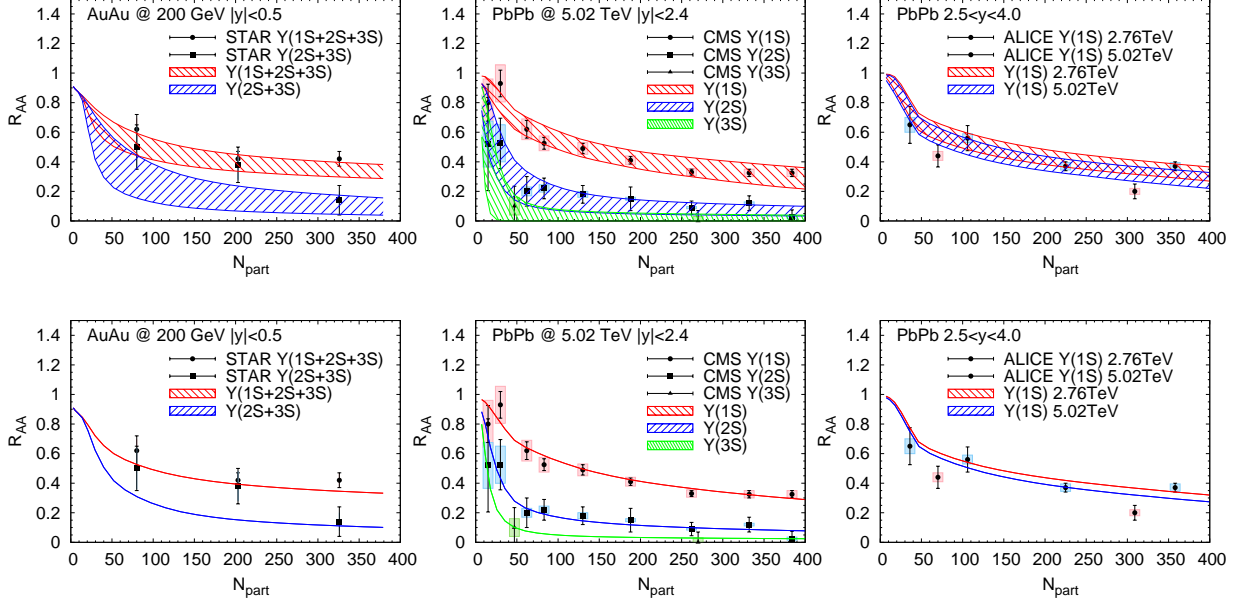


Figure 3: Bands of 95% confidence level (upper panels) and best-fit results (lower panels) for the $Y R_{AA}$'s in the $K=5$ scenario, compared to: $Y(1S+2S+3S)$ and $Y(2S+3S)$ STAR data in Au-Au(0.2 TeV) collisions (upper panels), $Y(1S, 2S, 3S)$ CMS data at mid-rapidity in PbPb(5.02 TeV) collisions (middle panels), and $Y(1S)$ ALICE data at forward rapidity in Pb-Pb(2.76, 5.02 TeV) collisions (lower panels).

For a given set of parameters, (a, b, c, d) , the dissociation energies of the different bottomonium states are calculated as a function of temperature, $E_D^Y(T; a, b, c, d)$, and the corresponding Y masses (figuring in the equilibrium limit, N_Y^{eq}) follow as

$$m_Y(T) = 2m_b(T) - E_D^Y(T). \quad (5)$$

With those inputs, we generate the reaction rates and evolve the Y numbers through the rate equation to compute a full set of Y nuclear modification factors,

$$R_{AA}^Y = \frac{N_{AA}^Y(N_{\text{part}})}{N_{\text{coll}}(N_{\text{part}})N_{pp}^Y}, \quad (6)$$

as a function of centrality (characterized by the number of nucleon participants, N_{part}) at RHIC ($\sqrt{s}=0.193, 0.2$ TeV) and the LHC ($\sqrt{s}=2.76, 5.02$ TeV, at both forward and mid-rapidity); $N_{AA}^Y(N_{\text{part}})$ denotes the final Y yield in an AA collision, which is normalized to its binary-collision number-scaled yield in pp collisions, $N_{\text{coll}}N_{pp}^Y$. As in our previous work [39] we utilize an entropy-conserving thermal fireball expansion (with a IQCD/hadron-resonance-gas equation of state) at each impact parameter and collision energy (which determine the total entropy via the observed charged-particle multiplicity). The initial Y numbers, $N_Y(\tau=0)$, in the rate equation (and the total $b\bar{b}$ number needed for the equilibrium limit, N_Y^{eq}) are determined from measured

Experiment	Rapidity	Data (R_{AA})	Reference
193 GeV U-U	$ y < 1.0$	1S, 1S+2S+3S	STAR [63]
200 GeV Au-Au	$ y < 0.5$	1S, 2S+3S, 1S+2S+3S	STAR [64]
2.76 TeV Pb-Pb	$ y < 2.4$	1S, 2S	CMS [35]
2.76 TeV Pb-Pb	$2.5 < y < 4.0$	1S	ALICE [65]
5.02 TeV Pb-Pb	$ y < 2.4$	1S, 2S, 3S	CMS [37]
5.02 TeV Pb-Pb	$2.5 < y < 4.0$	1S	ALICE [38]

Table 1: Summary of RHIC [63, 64] and LHC [35, 37, 38, 65] data utilized in our analysis.

cross sections in pp collisions, plus additional “cold-nuclear matter” (CNM) effects. Specifically, we employ baseline values for EPS09 nuclear shadowing [62] at the LHC of up to 15% and 30% in central collisions at mid and forward rapidity, respectively, and a nuclear absorption cross section of 3 mb at RHIC to account for the observed Y suppression in p -Au collisions. We have checked that upon reducing the CNM effects by a factor of 2, the overall fit quality worsens, with a thinner 95 % confidence level region and a slightly weaker extracted potential. Without CNM effects essentially no solutions were found within a 95 % confidence level.

For each parameter set, (a, b, c, d) , we evaluate the chi-squared as

$$\chi^2 = \sum_{i=1}^N \left(\frac{R_{AA}^{\text{mod}}(a, b, c, d) - R_{AA}^{\text{exp}}}{\sigma_{\text{exp}}} \right)^2, \quad (7)$$

Parameter	Range	Meaning
a	1.0-4.0	T slope of m_D
b	0.0-2.0	high- T slope of m_S
c	0.0-8.0	low- T slope of m_S
d	0.0-0.9	c -to- b transition region

Table 2: Summary of the $n=4$ fit parameters.

summed over $N=53$ experimental data points, R_{AA}^{exp} (cf. Tab. 1), and pertinent model values, R_{AA}^{mod} ; σ_{exp} denotes the quadratically combined $1\text{-}\sigma$ statistical and systematic experimental error,

$$\sigma_{\text{exp}} = \sqrt{\sigma_{\text{stat}}^2 + \sigma_{\text{sys}}^2}. \quad (8)$$

Assuming that a given model result represents the true values, and that the data are normal-distributed around these, the distribution of χ^2 values for given $\nu=N-n$, $\chi^2(\nu)$, is universal (and normalized) and can be used to define a confidence level. We employ a 95% confidence level which for $\nu=53-4=49$ implies χ^2 values below $\chi^2(49)=66.3$; this corresponds to an α -value of 0.05, *i.e.*, the integration of the χ^2 distribution above 66.3 yields 0.05, or: if the model is correct, there is only a 5% chance that the χ^2 -value is above 66.3.

The χ^2 values are computed over a grid of parameters (a, b, c, d) (cf. Tab. 2) which encompasses the minimum χ_{min}^2 representing the “best fit” and the 95 % confidence hypersurface defined by the maximal $\chi_{\text{max}}^2=66.3$. In between the grid points the results are emulated using a 4-dimensional quadratic interpolation mapped onto the R_{AA} values.

Open HF phenomenology in URHICs, especially the large elliptic flow observed for low-momentum D -mesons at both RHIC and the LHC, requires a large enhancement of the HQ thermalization rates over those obtained from pQCD Born diagrams [26]. Therefore, in addition to the baseline pQCD quasifree rate, we evaluate scenarios with a K factor of 5 and 10 in our statistical analysis (and explicitly show results for the former).

4. Potential Extraction

In Fig. 3 we summarize our fit results to $Y R_{AA}$ ’s for a selection of ALICE, CMS and STAR data for $K=5$; the bands agree well with the data. A very similar fit quality is achieved for $K=1$ and 10, with “best fit” results of $\chi_{\text{min}}^2 \approx 46$ for all cases. Because of this “degeneracy”, we do not need to treat K as an independent parameter. As in our previous work [39], we encounter significant discrepancies with the 2.76 TeV Pb-Pb forward-rapidity

data; when arbitrarily excluding them from the fit, the χ_{min}^2 drops from ~ 46 to ~ 35 .

Inspection of the parameter space in the (a, b) plane (Fig. 4) reveals a substantial shrinking of the 95 % confidence region of the T -dependence of the confining force (parameter b) as the heavy-light interaction strength (K factor) is increased. At moderate temperatures, the increase in the width caused by the K factor is compensated by a reduced screening to increase the dissociation energy and lower the final-state phase space. On the other hand, the screening of the color-Coulomb potential is not strongly constrained, characterized by a large range of values of the temperature slope, a , of m_D along a valley of $\chi^2/\nu \lesssim 1$. This finding highlights the sensitivity of bottomonium observables to the confining potential, which is also tightly connected to the strength of the heavy-light interaction. Without knowledge of the latter, it is difficult to draw definite conclusions.

The main transport parameter, the reaction rate, is shown in Fig. 5. The most relevant temperature region for phenomenology at RHIC and the LHC is $T \lesssim 400$ MeV since the fireball lifetime at higher temperature is (well) below 0.5 fm/c (based on our previous finding [39] that the $Y R_{AA}$ ’s are rather insensitive against variations in the initial QGP formation time, which controls the initial temperature; this is in part due to finite Y formation times). In this temperature range, the resulting $\Upsilon(1S)$ widths are very similar for $K=1$ and $K=5$; they also agree with the microscopic calculations in the T -matrix approach [18]. At higher temperature, the 95 % confidence bands become broad, but still have overlap until $T \approx 600$ MeV. The case could be made that this region can be probed rather sensitively in a future circular collider in the tens of TeV regime. On the other hand, the $\Upsilon(2S)$ rates differ largely beyond $T \approx 300$ MeV (reached after roughly 1 fm/c in central Pb-Pb collisions at the LHC), due to the different K factors at (near) vanishing dissociation energy. Again, this is somewhat mitigated by its finite formation time, but in any case, the $\Upsilon(2S)$ is highly suppressed in semi/central collisions (by 90% or more at the LHC) with a good fraction of the final yield due to regeneration which starts at $T \lesssim 250$ MeV, with then comparable rates for $K=1$ and $K=5$.

In Fig. 6 we display our main result, *i.e.*, the extracted in-medium HQ potentials at different temperatures for $K=1$ and 5. At low T , the potentials are close to the vacuum one in both scenarios, but for $K=5$ the potential remains substantially stronger at higher temperatures. Since the $K=1$ potential is incompatible with open HF phenomenology [12], the $K=5$ potential should be considered a much more realistic solution. Remarkably,

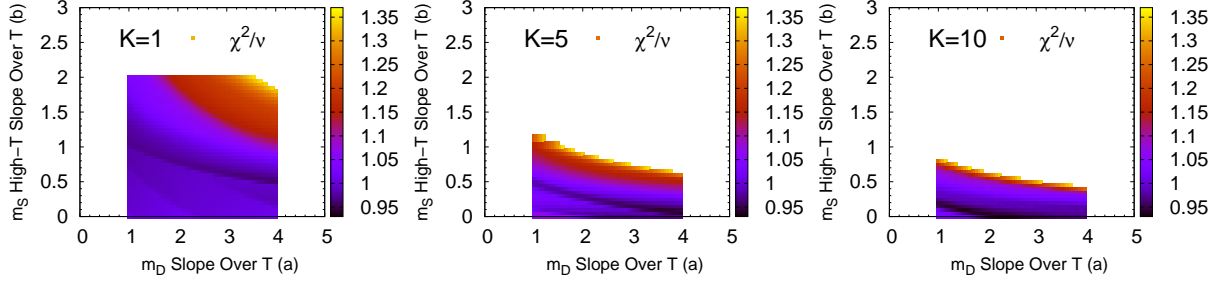


Figure 4: Color-coded χ^2/ν contours in the (a, b) parameter space (temperature slopes of string and Debye screening masses), projected to the minimum values in the associated (c, d) space, for $K=1$ (left), 5 (middle) and 10 (right).

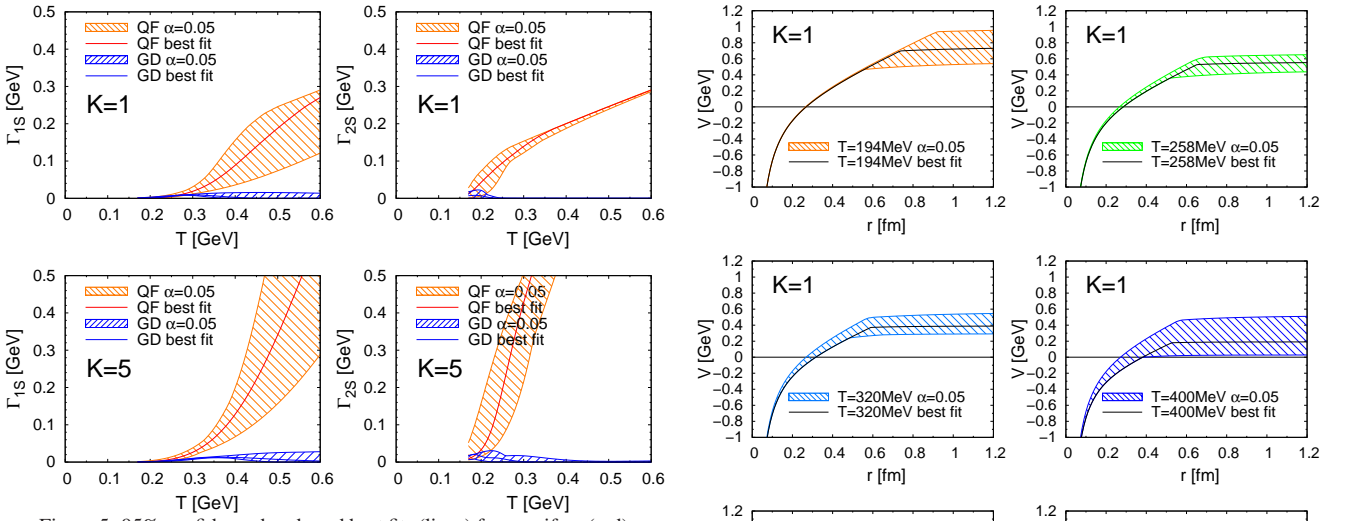


Figure 5: 95% confidence bands and best fits (lines) for quasifree (red) and gluo-dissociation (blue) rates for $Y(1S)$ (left panels) and $Y(2S)$ (right panels) for $K=1$ (upper panels) and $K=5$ (lower panels).

the latter closely coincides with the “strong-binding scenario” (with large E_D) in the microscopic T -matrix calculations of Ref. [18] which were only constrained by IQCD data (equation of state, quarkonium correlators and free energy), not by URHIC phenomenology.

5. Conclusions

Utilizing a well-tested quarkonium transport approach, we have conducted a statistical analysis to constrain the in-medium heavy-quark potential via bottomonium observables in heavy-ion collisions. The potential determines the in-medium Y dissociation energies, which in turn govern the reaction rate as the main transport coefficient. Guided by theoretical analyses of IQCD data on the HQ free energy, we have employed a 4-parameter ansatz to capture essential temperature effects on the color-Coulomb and string force components. As an important additional ingredient, we have

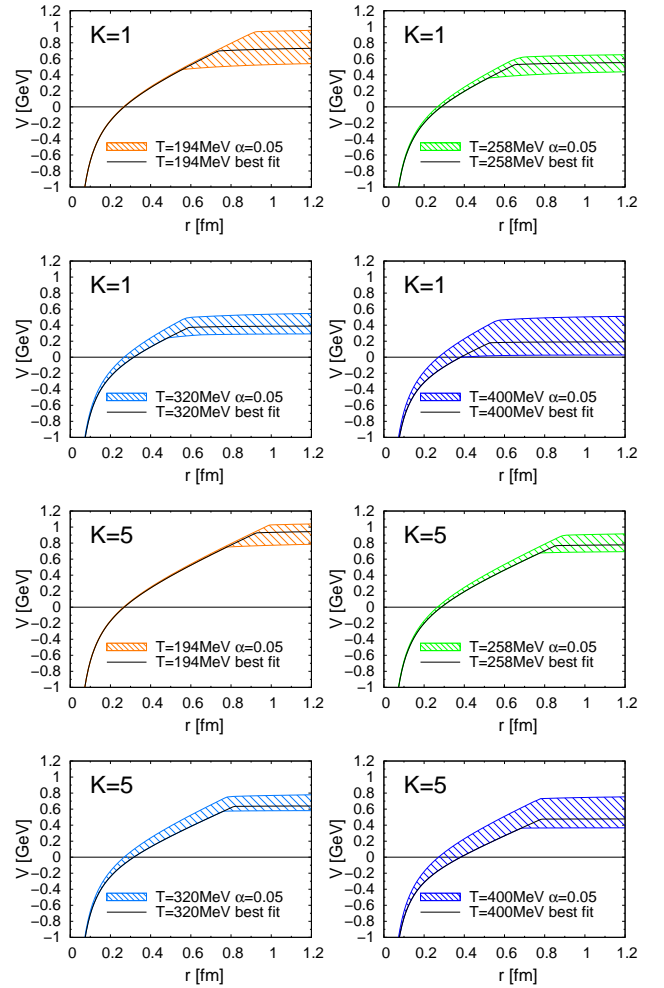


Figure 6: 95% confidence level bands for the extracted potential, $V(r) = V_{QQ}(r) - \frac{4}{3}\alpha_s m_D$, and the “best fits” (lines) at different temperatures for the $K=1$ (upper 2 rows) and $K=5$ (lower 2 rows) scenarios.

allowed for a nonperturbative enhancement in the bottomonium reaction rates. We have then constructed 95 % confidence regions of fits to R_{AA} data at RHIC

and the LHC to extract the in-medium potential for different K factors in the heavy-light interaction. The resulting reaction rates essentially coincide in the relevant temperature region, dictated by the transport fit to the data, but larger K factors lead to significantly stronger extracted potentials in the QGP. The stronger potentials, in turn, are required to obtain HQ transport coefficients that are viable for open HF phenomenology at RHIC and the LHC. Our approach thus highlights the importance of combined analyses of open and hidden HF probes in a microscopic calculation, and supports earlier independent findings that remnants of the confining force above T_{pc} are instrumental for the strong-coupling features of the QGP. Several improvements of our work are envisaged. Our previous checks of systematic uncertainties in the transport approach (including the bulk medium evolution, Y formation times and the impact of b -quark diffusion), should be revisited, together with explicit calculations of nonperturbative effects in the reaction rate [12, 18]. This may require the use of a quantum transport framework as currently being developed from several angles [48–52], as well as more advanced statistical tools to cope with an enlarged parameter space [66]. Extensions to the charmonium sector, where a rich data set is available, should also be pursued, posing additional challenges due to large regeneration contributions and the smaller charm-quark mass.

Acknowledgments

This work has been supported by the U.S. National Science Foundation under Grant No. PHY-1614484.

References

- [1] E. Eichten et al., Phys. Rev. Lett. 34 (1975) 369.
- [2] S. Godfrey and N. Isgur, Phys. Rev. D 32 (1985) 189.
- [3] W. Lucha, F.F. Schoberl and D. Gromes, Phys. Rept. 200 (1991) 127.
- [4] T. Matsui and H. Satz, Phys. Lett. B 178 (1986) 416.
- [5] L. Kluberg and H. Satz, Landolt-Bornstein 23 (2010) 373.
- [6] P. Braun-Munzinger and J. Stachel, Landolt-Bornstein 23 (2010) 424.
- [7] R. Rapp, D. Blaschke and P. Crochet, Prog. Part. Nucl. Phys. 65 (2010) 209.
- [8] A. Mocsy, P. Petreczky and M. Strickland, Int. J. Mod. Phys. A 28 (2013) 1340012.
- [9] R. Rapp and X. Du, Nucl. Phys. A967 (2017) 216.
- [10] H. van Hees et al., Phys. Rev. Lett. 100 (2008) 192301.
- [11] F. Riek and R. Rapp, Phys. Rev. C 82 (2010) 035201.
- [12] S.Y.F. Liu, M. He and R. Rapp, Phys. Rev. C99 (2019) 055201.
- [13] G.E. Brown et al., Nucl. Phys. A 740 (2004) 171.
- [14] E.V. Shuryak and I. Zahed, Phys. Rev. D 70 (2004) 054507.
- [15] M. Mannarelli and R. Rapp, Phys. Rev. C 72 (2005) 064905.
- [16] J. Liao and E. Shuryak, Phys. Rev. D 82 (2010) 094007.
- [17] S.Y.F. Liu and R. Rapp, (2016), 1612.09138.
- [18] S.Y.F. Liu and R. Rapp, Phys. Rev. C 97 (2018) 034918.
- [19] M. Laine et al., JHEP 0703 (2007) 054.
- [20] A. Beraudo, J.P. Blaizot and C. Ratti, Nucl. Phys. A 806 (2008) 312.
- [21] N. Brambilla et al., Phys. Rev. D 78 (2008) 014017.
- [22] A. Rothkopf, T. Hatsuda and S. Sasaki, Phys. Rev. Lett. 108 (2012) 162001.
- [23] Y. Burnier, O. Kaczmarek and A. Rothkopf, Phys. Rev. Lett. 114 (2015) 082001.
- [24] S.Y.F. Liu and R. Rapp, Nucl. Phys. A 941 (2015) 179.
- [25] A. Bazavov, Y. Burnier and P. Petreczky, Nucl. Phys. A 932 (2014) 117.
- [26] R. Rapp et al., Nucl. Phys. A979 (2018) 21.
- [27] X. Zhao and R. Rapp, Phys. Rev. C 82 (2010) 064905.
- [28] Y. Liu et al., Phys. Lett. B 697 (2011) 32.
- [29] A. Emerick, X. Zhao and R. Rapp, Eur. Phys. J. A 48 (2012) 72.
- [30] M. Strickland and D. Bazow, Nucl. Phys. A 879 (2012) 25.
- [31] K. Zhou, N. Xu and P. Zhuang, Nucl. Phys. A 931 (2014) 654.
- [32] STAR Collaboration, L. Adamczyk et al., Phys. Lett. B 735 (2014) 127, [Erratum: Phys. Lett. B743,537(2015)].
- [33] PHENIX Collaboration, A. Adare et al., Phys. Rev. C 91 (2015) 024913.
- [34] CMS Collaboration, S. Chatrchyan et al., Phys. Rev. Lett. 109 (2012) 222301, [Erratum: Phys. Rev. Lett. 120, no. 19, 199903 (2018)].
- [35] CMS Collaboration, V. Khachatryan et al., Phys. Lett. B 770 (2017) 357.
- [36] CMS Collaboration, A.M. Sirunyan et al., Phys. Rev. Lett. 120 (2018) 142301.
- [37] CMS Collaboration, A.M. Sirunyan et al., Phys. Lett. B 790 (2019) 270.
- [38] ALICE Collaboration, S. Acharya et al., Phys. Lett. B 790 (2019) 89.
- [39] X. Du, R. Rapp and M. He, Phys. Rev. C 96 (2017) 054901.
- [40] L. Grandchamp, R. Rapp and G.E. Brown, Phys. Rev. Lett. 92 (2004) 212301.
- [41] X. Zhao and R. Rapp, Nucl. Phys. A 859 (2011) 114.
- [42] E.G. Ferreira, Phys. Lett. B 731 (2014) 57.
- [43] K. Zhou et al., Phys. Rev. C 89 (2014) 054911, 1401.5845.
- [44] J. Hoelck, F. Nendzig and G. Wolschin, Phys. Rev. C 95 (2017) 024905.
- [45] B. Krouppa, A. Rothkopf and M. Strickland, Phys. Rev. D 97 (2018) 016017.
- [46] S. Aronson et al., Phys. Lett. B 778 (2018) 384.
- [47] E.G. Ferreira and J.P. Lansberg, JHEP 10 (2018) 094.
- [48] Y. Akamatsu, Phys. Rev. D 91 (2015) 056002.
- [49] R. Katz and P.B. Gossiaux, Annals Phys. 368 (2016) 267.
- [50] N. Brambilla et al., Phys. Rev. D 96 (2017) 034021.
- [51] J.P. Blaizot and M.A. Escobedo, Phys. Rev. D 98 (2018) 074007.
- [52] X. Yao and T. Mehen, Phys. Rev. D 99 (2019) 096028.
- [53] L. Grandchamp and R. Rapp, Phys. Lett. B 523 (2001) 60.
- [54] B.L. Combridge, Nucl. Phys. B 151 (1979) 429.
- [55] M.E. Peskin, Nucl. Phys. B 156 (1979) 365.
- [56] G. Bhanot and M.E. Peskin, Nucl. Phys. B 156 (1979) 391.
- [57] A. Mocsy and P. Petreczky, Phys. Rev. Lett. 99 (2007) 211602.
- [58] P. Petreczky and K. Petrov, Phys. Rev. D 70 (2004) 054503.
- [59] O. Kaczmarek, PoS CPOD07 (2007) 043.
- [60] A. Bazavov and P. Petreczky, J. Phys. Conf. Ser. 432 (2013) 012003.
- [61] A. Bazavov and P. Petreczky, Phys. Rev. D 87 (2013) 094505.
- [62] K.J. Eskola, H. Paukkunen and C.A. Salgado, JHEP 04 (2009) 065.
- [63] STAR Collaboration, L. Adamczyk et al., Phys. Rev. C 94

- (2016) 064904.
- [64] STAR Collaboration, Z. Ye, Nucl. Phys. A 967 (2017) 600.
 - [65] ALICE Collaboration, B.B. Abelev et al., Phys. Lett. B 738 (2014) 361.
 - [66] J.E. Bernhard et al., Phys. Rev. C 94 (2016) 024907.